

Discovery of a hyperluminous quasar at $z = 1.62$ with Eddington ratio > 3 in the eFEDS field confirmed by KOOLS-IFU on Seimei Telescope

Yoshiki TOBA^{1,2,3,4*,†}, Keito MASU², Naomi OTA², Zhen-Kai GAO^{3,5},
Masatoshi IMANISHI¹, Anri YANAGAWA², Satoshi YAMADA⁶, Itsuki
DOSAKA⁷, Takumi KAKIMOTO^{8,1}, Seira KOBAYASHI⁷, Neiro KUROKAWA²,
Aika OKI^{9,10}, Sorami SOGA², Kohei SHIBATA⁷, Sayaka TAKEUCHI²,
Yukana TSUJITA², Tohru NAGAO⁴, Masayuki TANAKA^{1,8}, Yoshihiro UEDA¹¹,
Wei-Hao WANG³

¹National Astronomical Observatory of Japan, 2-21-1 Osawa, Mitaka, Tokyo 181-8588, Japan

²Department of Physics, Nara Women's University, Kitauoyanishi-machi, Nara, Nara 630-8506, Japan

³Academia Sinica Institute of Astronomy and Astrophysics, 11F of Astronomy-Mathematics Building, AS/NTU, No.1, Section 4, Roosevelt Road, Taipei 10617, Taiwan

⁴Research Center for Space and Cosmic Evolution, Ehime University, 2-5 Bunkyo-cho, Matsuyama, Ehime 790-8577, Japan

⁵Graduate Institute of Astronomy, National Central University, 300 Zhongda Road, Zhongli, Taoyuan 32001, Taiwan

⁶RIKEN Cluster for Pioneering Research, 2-1 Hirosawa, Wako, Saitama 351-0198, Japan

⁷Department of Physics, Ehime University, 2-5 Bunkyo-cho, Matsuyama, Ehime 790-8577, Japan

⁸Department of Astronomical Science, The Graduate University for Advanced Studies, SOKENDAI, 2-21-1 Osawa, Mitaka, Tokyo 181-8588, Japan

⁹Department of Astronomy, Graduate School of Science, The University of Tokyo, 7-3-1 Hongo, Bunkyo-ku, Tokyo 113-0033, Japan

¹⁰Mizusawa VLBI Observatory, National Astronomical Observatory Japan, 2-21-1 Osawa, Mitaka, Tokyo 181-8588, Japan

¹¹Department of Astronomy, Kyoto University, Kitashirakawa-Oiwake-cho, Sakyo-ku, Kyoto 606-8502, Japan

*E-mail: yoshiki.toba@nao.ac.jp

Received 2024 April 28; Accepted 2024 August 11

Abstract

We report the discovery of a hyperluminous type 1 quasar (eFEDS J082826.9–013911; eFEDSJ0828–0139) at $z_{\text{spec}} = 1.622$ with a super-Eddington ratio (λ_{Edd}). We perform the optical spectroscopic observations with KOOLS-IFU on the Seimei Telescope. The black hole mass (M_{BH}) based on the single-epoch method with Mg II $\lambda 2798$ is estimated to be $M_{\text{BH}} = (6.2 \pm 1.2) \times 10^8 M_{\odot}$. To measure the precise infrared luminosity (L_{IR}), we obtain submillimeter data taken by SCUBA-2 on JCMT and conduct the spectral energy distribution analysis with X-ray to submillimeter data. We find that L_{IR} of eFEDSJ0828–0139 is $L_{\text{IR}} = (6.8 \pm 1.8) \times 10^{13} L_{\odot}$, confirming the existence of a hypeluminous infrared galaxy

(HyLIRG). λ_{Edd} is estimated to be $\lambda_{\text{Edd}} = 3.6 \pm 0.7$, making it one of the quasars with the highest BH mass accretion rate at cosmic noon.

Key words: quasars: individual (eFEDS J082826.9–013911) — quasars: supermassive black holes — infrared: galaxies

1 Introduction

It is widely accepted that almost all massive galaxies contain supermassive black holes (SMBHs) with a BH mass (M_{BH}) of $10^{5-10} M_{\odot}$ at the galaxy center and that their masses are strongly correlated with the mass of the spheroidal component of galaxies (e.g., Magorrian et al. 1998; Ferrarese & Merritt 2000; Marconi & Hunt 2003; Kormendy & Ho 2013; McConnell & Ma 2013). This suggests that the formation of SMBHs is closely related to the formation of galaxies, manifesting their co-evolution with host galaxies. However, the understanding of the co-evolution mechanism between the two, which differ by 9–10 orders of magnitude on the physical scale, has not been observationally constrained.

To address this issue, we focus on hyperluminous infrared galaxies (HyLIRGs) with an infrared (IR) luminosity (L_{IR}) of $> 10^{13} L_{\odot}$ (Rowan-Robinson 2000), most IR emission comes from hot dust heated by active galactic nuclei (AGNs) (e.g., Toba et al. 2015; Symeonidis & Page 2018). According to the galaxy and SMBH growth scenarios resulting from galaxy mergers expected from numerical simulations, HyLIRGs “theoretically” correspond to the most interesting phases in which the growth rates of galaxies and SMBH peak (e.g., Narayanan et al. 2010; Blecha et al. 2018; Yutani et al. 2022). Therefore, HyLIRGs are expected to serve as a crucial laboratory for probing the growth phase of co-evolution. However, AGN and host properties in HyLIRGs have still been poorly understood “observationally” because the number density of HyLIRGs is very small, and there have not been extensive multi-wavelength observations for them. To overcome this situation, deep and wide-field observation, particularly with X-ray data, is invaluable for uncovering the AGN properties of a spatially rare population, HyLIRGs, although X-ray observations of HyLIRGs are still limited (e.g., Wilman et al. 2003; Hlavacek-Larrondo et al. 2017; Ricci et al. 2017; Toba et al. 2020a; Toba et al. 2021b).

The advent of the eROSITA X-ray satellite (Merloni et al. 2012; Predehl et al. 2021) has enabled us to systematically investigate HyLIRGs from an AGN point of view because X-ray radiation is sensitive to finding AGNs. In this paper, we report the discovery of a hyperluminous quasar,

Table 1. Observed Properties of eFEDSJ0828–0139.

eFEDS J082826.9–013911	
ID_SRC (Brunner et al. 2022)	14050
SDSS ObjID	1237655176541241479
R.A. (LS8) [J2000.0]	08:28:27.145
Decl. (LS8) [J2000.0]	−01:39:12.18
Redshift (z_{spec})	1.6224 ± 0.0007
eROSITA $f_{2-10\text{keV}}$ [mJy]	$(8.83 \pm 3.64) \times 10^{-7}$
eROSITA $f_{0.5-2\text{keV}}$ [mJy]	$(4.06 \pm 1.67) \times 10^{-6}$
GALEX FUV [mJy]	$(1.13 \pm 0.45) \times 10^{-2}$
GALEX NUV [mJy]	$(7.13 \pm 0.73) \times 10^{-2}$
SDSS u -band [mJy]	$(2.54 \pm 0.04) \times 10^{-1}$
SDSS g -band [mJy]	$(5.32 \pm 0.02) \times 10^{-1}$
SDSS r -band [mJy]	$(7.64 \pm 0.03) \times 10^{-1}$
SDSS i -band [mJy]	$(8.84 \pm 0.04) \times 10^{-1}$
SDSS z -band [mJy]	$(8.45 \pm 0.09) \times 10^{-1}$
UKIDSS Y -band [mJy]	$(7.26 \pm 0.10) \times 10^{-1}$
UKIDSS J -band [mJy]	$(8.31 \pm 0.07) \times 10^{-1}$
UKIDSS H -band [mJy]	$(10.4 \pm 0.12) \times 10^{-1}$
UKIDSS K -band [mJy]	$(7.60 \pm 0.13) \times 10^{-1}$
WISE $3.4 \mu\text{m}$ [mJy]	$(11.4 \pm 0.05) \times 10^{-1}$
WISE $4.6 \mu\text{m}$ [mJy]	2.88 ± 0.12
WISE $12 \mu\text{m}$ [mJy]	3.30 ± 0.16
WISE $22 \mu\text{m}$ [mJy]	11.2 ± 1.29
AKARI $65 \mu\text{m}$ [Jy]	$< 1.44^*$
AKARI $90 \mu\text{m}$ [Jy]	$< 0.33^*$
AKARI $140 \mu\text{m}$ [Jy]	$< 0.84^*$
AKARI $160 \mu\text{m}$ [Jy]	$< 3.78^*$
SCUBA-2/JCMT $450 \mu\text{m}$ [mJy]	$< 44.6^*$
SCUBA-2/JCMT $850 \mu\text{m}$ [mJy]	$< 5.90^*$
$E(B-V)^*$	$(1.3 \pm 0.4) \times 10^{-1}$
M_* [M_{\odot}]	$(3.9 \pm 2.0) \times 10^{11}$
SFR [$M_{\odot} \text{ yr}^{-1}$]	$(1.3 \pm 0.5) \times 10^3$
L_{IR} [L_{\odot}]	$(6.8 \pm 1.8) \times 10^{13}$
$L_{\text{bol}}^{\text{AGN}}$ [erg s^{-1}]	$(2.9 \pm 0.1) \times 10^{47}$
M_{BH} [M_{\odot}]	$(6.2 \pm 1.2) \times 10^8$
λ_{Edd}	3.6 ± 0.7

The SDSS ObjID is valid for SDSS Data Release 8 or later. All the flux densities from X-ray (eROSITA) to mid-IR (WISE) are corrected for Galactic extinction.

* 3σ upper limits.

eFEDS J082826.9–013911 (hereafter, eFEDSJ0828–0139), at $z_{\text{spec}} = 1.622$ with a super-Eddington ratio of $\lambda_{\text{Edd}} > 3.0$. Table 1 summarizes complete information, including photometry on this object and its physical properties obtained in this work. This is confirmed by (i) optical spectroscopic observations with the Kyoto Okayama

[†] NAOJ fellow

Optical Low-dispersion Spectrograph with optical fiber IFU (KOOLS-IFU: Yoshida 2005; Matsubayashi et al. 2019) on the Seimei Telescope (Kurita et al. 2020), and (ii) multi-wavelength data analysis from X-ray to submillimeter. In particular, because IFU data mitigate slit-loss of flux, unlike single-fiber or -slit spectroscopy, our KOOLS-IFU observation benefits not just extended sources like nearby galaxies (e.g., Toba et al. 2022a) but also point sources like AGNs (e.g., Hoshi et al. 2024).

The remainder of this paper is structured as follows. We describe target selection and follow-up observations using optical spectroscopy and submillimeter imaging in section 2. The derived AGN and host properties with their potential uncertainties and the characterization of eFEDSJ0828–0139 are presented in section 3. We summarize the results of this work in section 4. This work assumes a flat Universe with $H_0 = 70 \text{ km s}^{-1} \text{ Mpc}^{-1}$, $\Omega_M = 0.3$, and $\Omega_\Lambda = 0.7$.

2 Data and analysis

2.1 Sample selection

The target (eFEDSJ0828–0139) was selected from the HyLIRG candidate sample provided by Toba et al. (2022b). A full description of HyLIRG candidate selection is presented by Y. Toba et al. (in preparation). Hence, we present a summary. Toba et al. (2022b) performed the spectral energy distribution (SED) analysis for Wide-field Infrared Survey Explorer (WISE: Wright et al. 2010) 22 μm -selected sources in the eROSITA Final Equatorial Depth Survey (eFEDS: Brunner et al. 2022). According to their L_{IR} , 150 HyLIRG candidates were left, more than half of which have spectroscopic redshift (z_{spec}) through the follow-up campaign, such as the Sloan Digital Sky Survey (SDSS; York et al. 2000) V/eFRDS observations (Almeida et al. 2023).

Our target is the brightest source in the optical (r -mag = 16.78) among our HyLIRG candidate sample with photometric redshift (z_{phot}). eFEDSJ0828–0139 is classified as an unobscured AGN (i.e., quasar) with a hydrogen column density of $\log N_{\text{H}} \sim 20.8 \text{ cm}^{-2}$ through an eROSITA spectral analysis (Liu et al. 2022). This object has also been selected as an AGN/quasar candidate from a multi-wavelength photometric perspective, such as WISE (Secrest et al. 2015; Assef et al. 2018) and Gaia (Bailer-Jones et al. 2019; Wu et al. 2023). Its z_{phot} is estimated by some studies, for instance, $z_{\text{phot}} = 2.825^{+0.405}_{-0.215}$ (Richards et al. 2015), 1.321 ± 0.611 (Duncan 2022) and $1.367^{+0.192}_{-0.126}$ (Salvato et al. 2022), indicating a large redshift uncertainty.

Table 2. Observation log in 2023A and 2023B semester.

Observing date	Grism	Exposure time (s)	Standard star
Jan. 25, 2023	VPH-blue	7200	HR1544
Jan. 27, 2023	VPH-blue	3600	HD74280
Feb. 13, 2023	VPH-blue	600	HD74280
Dec. 12, 2023	VPH-blue	4200	HD74280

2.2 Observations and data reduction

2.2.1 KOOLS-IFU on Seimei telescope

To measure z_{spec} and BH properties, we observed eFEDSJ0828–0139 with the KOOLS-IFU on the Seimei Telescope in 2023 (PI: Y.Toba with proposal IDs = 23A-N-CN01 and 23B-N-CN07). The Seimei Telescope is a 3.8-meter diameter optical-IR alt-azimuth mount telescope located at Okayama Observatory, Kyoto University, Okayama Prefecture in Japan, where the typical seeing on this site is $1.2''$ – $1.4''$. The KOOLS-IFU comprises 117 fibers with a total field of view (FoV) of $8.4'' \times 8.0''$. We used the VPH-blue² among four grisms equipped with KOOLS-IFU. The wavelength coverage is 4100–8900 Å and the spectral resolution ($R = \lambda/\Delta\lambda$) is approximately 500. The observational log is summarized in Table 2. The total integration time is approximately 4.3 hours.

We note that our target is well-fitted by a round exponential galaxy model (REX³) rather than a point spread function (PSF) model according to the DESI Legacy Imaging Survey catalog (Dey et al. 2019), which could indicate that the target is a slightly extended source. The Petrosian (Petrosian 1976) radius in r -band is 1.99 ± 0.01 arcsec (see `PhotoObj` table in the SDSS). Hence, our target would benefit from an IFU observation to mitigate flux loss.

The data reduction was executed with the Image Reduction and Analysis Facility (IRAF: Tody 1986) and the pipeline tools⁴ dedicated to the KOOLS-IFU. This procedure includes overscan subtraction, bad column correction, bias subtraction, flat fielding, wavelength calibration, spectral extraction, sky subtraction, flux calibration, and making a spectrum by combining spectra from all fibers on which the object is located. Ne, Hg, and Xe lamp data were used for wavelength calibration. We took a weighted mean of the spectra taken each day to obtain a spectrum with a high signal-to-noise (SN) ratio. Possible flux loss was corrected by scaling the spectrum to match the SDSS r -band magnitude.

¹ The configuration of KOOLS-IFU (such as number of fibers) was updated in October 2020.

² <http://www.o.kwasan.kyoto-u.ac.jp/inst/p-kools/performance/>

³ <https://www.legacysurvey.org/dr8/catalogs/#goodness-of-fits-and-morphological-type>

⁴ We downloaded a package on April 11, 2024 (see <http://www.kuastro.kyoto-u.ac.jp/~iwamuro/KOOLS/>).

2.2.2 SCUBA-2 on JCMT

In Toba et al. (2022b), the far-IR (FIR) and submillimeter data for eFEDSJ0828–0139 were lacking, and only AKARI FIR (shallow) upper limits were provided. Because the submillimeter data are crucial for precise measurement of L_{IR} (Toba et al. 2018; Toba et al. 2020c), we observed eFEDSJ0828–0139 with the Submillimetre Common User Bolometer Array 2 (SCUBA-2: Holland et al. 2013) on the James Clerk Maxwell Telescope (JCMT), providing 450 and 850 μm photometry. Our observation was executed under the Band-1 condition ($\tau_{225\text{GHz}} < 0.05$) on January 23, 2024, through a 24A regular program (M24AP001, PI: Y.Toba). The total on-source integration time is about 1 hour, twice the 30-minute scans by the compact ‘‘Daisy’’ scan pattern. During the observations, we observed a nearby radio source, 0828+046, for a pointing check. Data reduction and flux measurements at 450 and 850 μm were performed in a standard manner (e.g., Wang et al. 2017; Lim et al. 2020; Gao et al. 2024) with the aid of the Sub-Millimeter Common User Reduction Facility (Chapin et al. 2013) and the Pipeline for Combining and Analyzing Reduced Data (PICARD: Jenness et al. 2008). A full description of SCUBA-2 data reduction and flux measurements will be provided in Y.Toba et al. (in preparation)⁵.

2.3 Spectral fitting

To derive AGN properties such as AGN bolometric luminosity ($L_{\text{bol}}^{\text{AGN}}$), M_{BH} , and λ_{Edd} of our quasar, spectral fitting to KOOLS-IFU spectrum was conducted using the Quasar Spectral Fitting package (QSFIT v1.3.0⁶: Calderone et al. 2017). We fitted the KOOLS-IFU spectrum as a combination of (i) an AGN continuum with a single power-law, (ii) a Balmer continuum modeled by Grandi (1982) and Dietrich et al. (2002), (iii) iron-blended emission lines with UV-optical templates (Véron-Cetty et al. 2004; Vestergaard & Wilkes 2001), and (iv) emission lines with Gaussian components. QSFIT fits all the components simultaneously following a Levenberg-Marquardt least-squares minimization algorithm with MPFIT (Markwardt 2009) procedure. Spectral fitting was executed after correcting for the galactic extinction provided by Schlegel et al. (1998) with the Milky Way attenuation curve (O’Donnell 1994).

The main purpose of this spectral fitting is to measure the full width at half maximum (FWHM) of Mg II $\lambda 2798$

and continuum luminosity at 3000 \AA , $\lambda L_{\lambda}(3000 \text{\AA})$, that are ingredients for M_{BH} estimates. Based on outputs from QSFIT, we estimated M_{BH} through a single-epoch recipe provided by Vestergaard & Osmer (2009);

$$M_{\text{BH}}[M_{\odot}] = 10^{6.86} \left[\frac{\text{FWHM}(\text{MgII})}{1000 \text{ km s}^{-1}} \right]^2 \left[\frac{\lambda L_{\lambda}(3000 \text{\AA})}{10^{44} \text{ erg s}^{-1}} \right]^{0.5}. \quad (1)$$

$L_{\text{bol}}^{\text{AGN}}$ was converted from $\text{BC}_{3000} \times \lambda L_{\lambda}(3000 \text{\AA})$ where $\text{BC}_{3000} = 5.2 \pm 0.2$ is the bolometric correction (Runnoe et al. 2012). Following Toba et al. (2021a), the uncertainty in M_{BH} is calculated through the error propagation of Equation 1 while the uncertainty in $L_{\text{bol}}^{\text{AGN}}$ is propagated from 1σ errors of $\lambda L_{\lambda}(3000 \text{\AA})$ and BC_{3000} .

2.4 SED fitting

We collected the multi-wavelength data from X-ray to FIR in the same manner as Toba et al. (2022b). We refer the reader to that paper for details, but in short, we used GALEX (Martin et al. 2005) for ultraviolet (UV) data, SDSS for optical data, UKIDSS (Lawrence et al. 2007) for near-IR (NIR) data, WISE for mid-IR (MIR) data, and AKARI (Murakami et al. 2007) for FIR data. UV-to-MIR photometry is corrected for Galactic extinction (Schlegel et al. 1998). In addition, we have added photometry obtained from SCUBA-2 observation (section 2.2.2). Because our target was not detected at 450 and 850 μm , we input their 3σ upper limits for the SED fitting, which is crucial to pin down the FIR SED of eFEDSJ0828–0139.

We employed the Code Investigating GALaxy Emission (CIGALE ver.2022.1⁷; Burgarella et al. 2005; Noll et al. 2009; Boquien et al. 2019; Yang et al. 2020; Yang et al. 2022). This code allows us to include values for many parameters related to, e.g., the star formation (SF) history (SFH), single stellar population (SSP), attenuation law, AGN emissions, and dust emissions by considering the energy balance between the UV/optical and IR (see, e.g., Hashiguchi et al. 2023; Toba et al. 2024). Table 3 summarizes the parameter ranges used in the SED fitting with CIGALE. These parameter sets are the same as presented in Toba et al. (2021b) optimized for HyLIRG candidates. A full description of the assumed models is provided by Toba et al. (2021b); hence, we provide a summary. We assume a delayed SFH with recent starburst (Ciesla et al. 2017) with parameterizing e-folding time of the main stellar population model (τ_{main}), the age of the main stellar population in the galaxy, the age of the burst, and the ratio of the SF rate (SFR) after and before the burst (R_{sfr}). A starburst attenuation curve (Calzetti et al. 2000; Leitherer et al. 2002) is used for dust attenuation, in which we parameterize the

⁵ Our observations aim at observing seven HyLIRG candidates, including eFEDSJ0828–0139, which will be presented once observations are completed.

⁶ <https://qsfit.inaf.it>

⁷ <https://cigale.lam.fr/2022/07/04/version-2022-1/>

Table 3. Parameter values used in SED fitting with CIGALE

Parameter	Value
Delayed SFH with recent starburst (Ciesla et al. 2017)	
τ_{main} [Gyr]	1.0, 4.0, 8.0, 12
age [Gyr]	0.5, 1.0, 1.5, 2.0
age of burst [Myr]	10, 50, 100
R_{sfr}	1, 5, 10
SSP (Bruzual & Charlot 2003)	
IMF	Chabrier 2003
Metallicity	0.02
Nebular emission (Inoue 2011)	
$\log U$	-3.0, -2.0, -1.0
Dust attenuation (Calzetti et al. 2000; Leitherer et al. 2002)	
$E(B-V)_{\text{lines}}$	0.0, 0.1, 0.2, 0.3, 0.4, 0.5, 1.0
AGN Emission (Stalevski et al. 2012; Stalevski et al. 2016)	
$\tau_{9.7}$	3, 7, 11
p	0.5, 1.5
q	0.5, 1.5
Δ [°]	40
$R_{\text{max}}/R_{\text{min}}$	30
θ [°]	0, 10, 20
f_{AGN}	0.4, 0.5, 0.6, 0.7, 0.8, 0.9
Dust Emission (Draine et al. 2014)	
q_{PAH}	2.50, 5.26, 6.63, 7.32
U_{min}	10.0, 50.0
α	1.0, 1.5, 2.0
γ	0.01, 0.1, 1.0
X-ray Emission (Yang et al. 2022)	
AGN photon index (Γ)	2.0
α_{OX}	-2.0, -1.9, -1.8, -1.7
$ \Delta\alpha_{\text{OX}} _{\text{max}}$	0.5

color excess of the nebular emission lines, $E(B-V)_{\text{lines}}$. We chose the SSP model (Bruzual & Charlot 2003), assuming the initial mass function (IMF) of Chabrier 2003, and the standard nebular emission model with the implementation of the new CLOUDY HII-region model (Villa-Vélez et al. 2021) is included in CIGALE (Inoue 2011). AGN emission is modeled by using the SKIRTOR (Stalevski et al. 2016). This torus model consists of seven parameters: torus optical depth at $9.7 \mu\text{m}$ ($\tau_{9.7}$), torus density radial parameter (p), torus density angular parameter (q), the angle between the equatorial plane and edge of the torus (Δ), the ratio of the maximum to minimum radii of the torus ($R_{\text{max}}/R_{\text{min}}$), viewing angle (θ), and AGN fraction in total IR luminosity (f_{AGN}). Dust grain emission is modeled by Draine et al. (2014) in which we parameterize the mass fraction of PAHs (q_{PAH}), the minimum radiation field (U_{min}), the power-low slope of the radiation field distribution (α), and the fraction illuminated with a variable radiation field ranging from U_{min} to U_{max} (γ). X-ray emission is modeled with a fixed power-law photon index of AGN (Liu et al. 2022), and only α_{OX} is parameterized.

3 Results and discussion

3.1 Results of spectral fitting and AGN properties

Figure 1 shows the optical spectrum of eFEDSJ0828–0139 taken by the KOOLS-IFU, where several emission lines such as Al III λ 1860, Si III λ 1892, C III λ 1909 and Mg II are clearly detected. The result of the spectral fitting with QSFIT is also shown in Figure 1. The spectroscopic redshift of eFEDSJ0828–0139 measured from Mg II is $z_{\text{spec}} = 1.6224 \pm 0.0007$. The FWHM of Mg II and the continuum luminosity at 3000 \AA are $\text{FWHM}(\text{Mg II}) = (1.9 \pm 0.2) \times 10^3 \text{ km s}^{-1}$ and $\lambda L_{\lambda}(3000 \text{ \AA}) = (56.1 \pm 0.4) \times 10^{45} \text{ erg s}^{-1}$, respectively, which results in the black hole mass of $M_{\text{BH}} = (6.2 \pm 1.2) \times 10^8 M_{\odot}$. We note that Buendia-Rios et al. (2023) recently provided a recipe for virial BH mass based on Al III line. We find that the BH mass using their recipe is $\log(M_{\text{BH}}^{\text{Al III}}/M_{\odot}) \sim 8.5$, which is roughly consistent with Mg II-based M_{BH} . Eddington luminosity is $L_{\text{Edd}} = (8.0 \pm 0.2) \times 10^{46} \text{ erg s}^{-1}$. The AGN bolometric luminosity is $L_{\text{bol}}^{\text{AGN}} = (2.9 \pm 0.1) \times 10^{47} \text{ erg s}^{-1}$, indicating a hyper-luminous quasar as similar to WISE-SDSS selected, WISSH quasars at $z > 2$ (Duras et al. 2017). Consequently, the Eddington ratio of eFEDSJ0828–0139 is estimated to be $\lambda_{\text{Edd}} = 3.6 \pm 0.7$, making it a prominent quasar with BH at super-Eddington accretion.

Martínez-Aldama et al. (2018) reported that such quasars with extremely-high λ_{Edd} (so-called extreme accretor (xA) quasars: Marziani & Sulentic 2014) shows relatively strong Al III and Si III] emissions compared with C III] and conspicuous Fe II lines in their rest UV-to-optical spectra. We find that the line flux ratio for Al III/Si III] and C III]/Si III] is 0.44 ± 0.18 and 1.25 ± 0.27 , respectively. These values satisfy the selection criteria of xA quasars (Marziani & Sulentic 2014), supporting that eFEDSJ0828–0139 is an extremely high λ_{Edd} quasar.

A caveat is that BH mass estimated by a single-epoch method (i.e., Equation 1) has a sizeable systematic uncertainty up to 0.4 dex (see, e.g., Shen 2013), which has also been supported by the recent reverberation mapping with the SDSS (Shen et al. 2024). This means that the estimated Eddington ratio also potentially has a large uncertainty. We confirm the estimated BH mass is consistent with that using another emission line (albeit a single epoch) and obtain evidence of a high Eddington ratio inferred from emission line ratios. However, our M_{BH} and λ_{Edd} do not include the systematic errors mentioned above, which should be kept in mind for the following discussion.

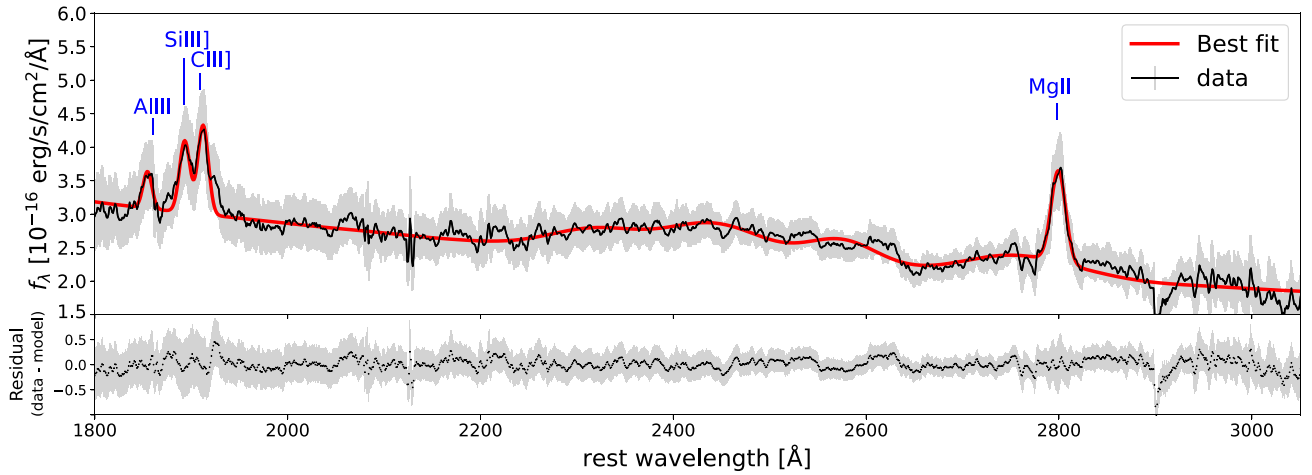


Fig. 1. The optical spectrum of eFEDSJ0828–0139 taken by the KOOLS-IFU. The black and gray lines represent observed data and its 1σ uncertainty. Blue vertical lines and labels mark detected lines. The best-fit line by `qsfFit` is shown with the red line. The bottom panel shows the residual (data – model) with 1σ uncertainty. Note that there is a relatively large residual around rest-frame ~ 2900 Å (observed-frame 7500 Å). This is due to the strongest telluric absorption line by O_2 (A-band) in the observed wavelength (Rudolf et al. 2016).

3.2 Results of SED fitting and AGN host properties

Figure 2 shows the best-fit SED of eFEDSJ0828–0139, demonstrating that the observed SED is moderately well-fitted by the stellar, nebular, AGN, and SF components with a reduced χ^2 of 4.9. The derived total IR luminosity is $L_{\text{IR}} = (6.8 \pm 1.8) \times 10^{13} L_{\odot}$, which confirms that our target is an HyLIRG. The stellar mass (M_*) and star formation rate (SFR) are $M_* = (3.9 \pm 2.0) \times 10^{11} M_{\odot}$ and $\text{SFR} = (1.3 \pm 0.5) \times 10^3 M_{\odot} \text{ yr}^{-1}$, respectively. These are typical values of HyLIRGs reported in previous works (e.g., Gao et al. 2021). The BH mass and stellar mass ratio of eFEDSJ0828–0139 is $\log(M_{\text{BH}}/M_*) = -2.8 \pm 0.2$, which agrees with the results reported in Suh et al. (2020).

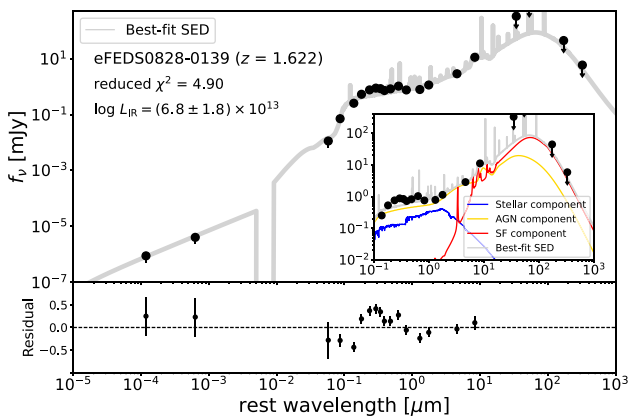


Fig. 2. Best-fit SED of eFEDSJ0828–0139. The black points are the photometric data, and the solid gray line represents the resultant best-fit SED. The inset figure shows the SED at $0.1\text{--}1000 \mu\text{m}$, where the contributions from the stellar, nebular, AGN, and SF components to the total SED are shown as blue, green, yellow, and red lines, respectively. Relative residual (defined as $(\text{data} - \text{best-fit})/\text{data}$) are shown at the bottom, where the black line represents the case in which the residual is zero.

3.3 Potential uncertainties on IR luminosity and SFR

A potential issue caused by the SED fitting with upper limits of AKARI and SCUBA-2 data is about SF (i.e., dust emission from host galaxy) contribution to the total SED, which is also relevant to the accuracy of IR luminosity and SFR. The `CIGALE` takes into account energy conservation of the amount of UV/optical radiation from SF and AGN absorbed by a dust and the amount of IR radiation re-emitted by the dust when the SED fitting. Hence, FIR SED is expected to be constrained reasonably. Nevertheless, the lack of deep FIR data around the peak of the FIR SED would affect the results. To test the requirement to add an SF component to the SED fitting, we employ the Bayesian information criterion (BIC; Schwarz 1978) for two fits that are derived with and without an SF component. The BIC is defined as $\text{BIC} = \chi^2 + k \times \ln(n)$, where χ^2 is non-reduced chi-square, k is the number of degrees of freedom (DOF), and n is the number of photometric data points used for the fitting, respectively. We then compare the results of two SED fittings without/with the SF (dust emission) module by using $\Delta\text{BIC} = \text{BIC}_{\text{w/oSF}} - \text{BIC}_{\text{w/SF}}$. The ΔBIC tells whether the SF/dust model is needed to provide a better fit by considering the difference in DOF (e.g., Ciesla et al. 2017; Buat et al. 2019; Aufort et al. 2020; Toba et al. 2020b). If ΔBIC is larger than two, adding the SF/dust component provides a better fit than not (Liddle 2004; Stanley et al. 2015). The resultant value for eFEDSJ0828–0139 is $\Delta\text{BIC} = 7.3$, which suggests that the SF/dust component is required to explain the observed SED.

We also estimate IR luminosity and SFR based on the SED fitting without using SCUBA-2 data to see how even

the upper limits of SCUBA-2 data are crucial to constrain those quantities. The resultant values are $L_{\text{IR}} = (7.3 \pm 1.9) \times 10^{13} L_{\odot}$ and $\text{SFR} = (1.6 \pm 0.6) \times 10^3 M_{\odot} \text{ yr}^{-1}$, which suggests that SCUBA-2 data prevents SFR and L_{IR} from being overestimated. In summary, dust emission from the host galaxy requires explaining the observed SED, and SCUBA-2 data are crucial to pin down the FIR SED, even if they are upper limits. Hence, potential uncertainties on IR luminosity and SFR are expected to be small in this work.

3.4 Characterization of eFEDSJ0828–0139

Figure 3 shows the Eddington ratio as a function of redshift. We compare the Eddington ratio from a value-added catalog⁸ (Wu & Shen 2022) for the SDSS DR16 quasar catalog (Lyke et al. 2020), in which the continuum and emission-line properties for 750,414 broad-line quasars are provided. Note that 25 sources have $\lambda_{\text{Edd}} > 3$ among the quasars with $1 < z < 2$. We visually check their spectra and find that the Eddington ratios of the majority of these quasars are poorly constrained with a large uncertainty of λ_{Edd} ($\sigma_{\lambda_{\text{Edd}}}$) partially due to the low SN of the emission lines (C IV and Mg II). If we restrict ourselves to $\lambda_{\text{Edd}}/\sigma_{\lambda_{\text{Edd}}} > 5$ (that is similar to eFEDSJ0828–0139), only four objects remain. We also compare λ_{Edd} of WISSH quasars (Vietri et al. 2018) and extremely red quasars (ERQs: Perrotta et al. 2019) that are also known as high λ_{Edd} quasars.

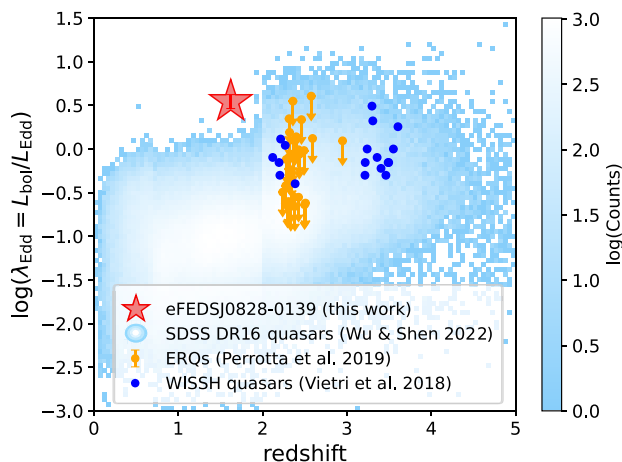


Fig. 3. Eddington ratio as a function of redshift. The red star represents eFEDSJ0828–0139. The blue 2D histogram represents the number density of SDSS DR16 quasars (Wu & Shen 2022). Quasars with $\lambda_{\text{Edd}}/\sigma_{\lambda_{\text{Edd}}} > 5$ are plotted. The blue and orange circles represent ERQs (Perrotta et al. 2019) and WISSH quasars (Vietri et al. 2018), respectively.

We find that eFEDSJ0828–0139 has the highest λ_{Edd}

⁸ http://quasar.astro.illinois.edu/paper_data/DR16Q/dr16q_prop_May16_2023.fits.gz

at $z \sim 1.6$, which is even higher than the ERQs and WISSH quasars at $z > 2$. In addition to a high BH accretion rate, this object has an extremely high SFR ($> 1000 M_{\odot} \text{ yr}^{-1}$) as described in section 3.2. Given the fact that M_{BH}/M_{\star} value is consistent with local relation (Suh et al. 2020), we may be witnessing the growing phase of both SMBH and its host galaxy in the course of the galaxy–SMBH co-evolution, as expected by the numerical simulation.

4 Summary

This work presents the hyper-luminous IR galaxy, eFEDSJ0828–0139, discovered by eROSITA. To characterize this HyLIRG candidate, we perform the optical spectroscopy with KOOLS-IFU on the Seimei Telescope and sub-mm imaging with SCUBA-2 on JCMT. From KOOLS-IFU observations, its spectroscopic redshift is measured to be $z_{\text{spec}} = 1.622$. We evaluate BH mass based on the single epoch method with Mg II line and IR luminosity based on the SED fitting. With the caveat of the potential uncertainty of the derived physical properties discussed in sections 3.1 and 3.3, we find that IR luminosity of eFEDSJ0828–0139 is $L_{\text{IR}} = (6.8 \pm 1.8) \times 10^{13} L_{\odot}$ and Eddington ratio is $\lambda_{\text{Edd}} = 3.6 \pm 0.7$, confirming an HyLIRG with SMBH being super-Eddington accretion. Its SFR is also high, $(1.3 \pm 0.5) \times 10^3 M_{\odot} \text{ yr}^{-1}$. These results indicate that eFEDSJ0828–0139 is in a particular phase in which SMBH and its host galaxy are actively growing in the framework of galaxy–SMBH co-evolution.

Although this paper reports only one HyLIRG in the eFEDS region, several thousands of HyLIRG candidates can be selected with the aid of the eROSITA all-sky survey (Merloni et al. 2024). Spectroscopic follow-up observations with next-generation multiobject spectrographs, such as the Subaru Prime Focus Spectrograph (PFS; Takada et al. 2014; Greene et al. 2022) provide an essential benchmark for the forthcoming systematic HyLIRG survey with eROSITA.

Acknowledgments

We acknowledge an anonymous referee for valuable suggestions that improved the paper. We thank Drs. Masafusa Onoue and Akatoki Noboriguchi for their support in data analysis. We also thank Dr. Fumihide Iwamuro for developing a data reduction pipeline for KOOLS-IFU. We are grateful to Yumiko Anraku, Yurika Matsuo, Arisa Yoshino, and the staff of the Okayama Astrophysical Observatory, a branch of the National Astronomical Observatory of Japan, for their support during our observations. Data reduction for KOOLS-IFU was carried out on the Multi-wavelength Data Analysis System operated by the Astronomy Data Center (ADC), National Astronomical Observatory of Japan.

This work is based on data from eROSITA, the soft X-ray instrument aboard SRG, a joint Russian-German science mission supported by the Russian Space Agency (Roskosmos), in the interests of the Russian Academy of Sciences represented by its Space Research Institute (IKI), and the Deutsches Zentrum für Luft- und Raumfahrt (DLR). The SRG spacecraft was built by Lavochkin Association (NPOL) and its subcontractors, and is operated by NPOL with support from the Max Planck Institute for Extraterrestrial Physics (MPE). The development and construction of the eROSITA X-ray instrument was led by MPE, with contributions from the Dr. Karl Remeis Observatory Bamberg & ECAP (FAU Erlangen-Nuernberg), the University of Hamburg Observatory, the Leibniz Institute for Astrophysics Potsdam (AIP), and the Institute for Astronomy and Astrophysics of the University of Tübingen, with the support of DLR and the Max Planck Society. The Argelander Institute for Astronomy of the University of Bonn and the Ludwig Maximilians Universität Munich also participated in the science preparation for eROSITA.

The James Clerk Maxwell Telescope is operated by the East Asian Observatory on behalf of The National Astronomical Observatory of Japan; Academia Sinica Institute of Astronomy and Astrophysics; the Korea Astronomy and Space Science Institute; the National Astronomical Research Institute of Thailand; Center for Astronomical Mega-Science (as well as the National Key R&D Program of China with No. 2017YFA0402700). Additional funding support is provided by the Science and Technology Facilities Council of the United Kingdom and participating universities and organizations in the United Kingdom and Canada. Additional funds for the construction of SCUBA-2 were provided by the Canada Foundation for Innovation.

This work is supported by JSPS KAKENHI Grant numbers JP22H01266 and JP23K22537 (Y.T.), JP20K04027 (N.O.), and JP21K03632 (M.I.). Z.K.G. and W.H.W. acknowledge support from the National Science and Technology Council of Taiwan (NSTC 111-2112-M-001-052-MY3).

References

- Almeida, A. et al. 2023, *ApJS*, 267, 2, 44
- Assef, R. J., Stern, D., Noirot, G., Jun, H. D., Cutri, R. M., & Eisenhardt, P. R. M. 2018, *ApJS*, 234, 2, 23
- Aufort, G., Ciesla, L., Pudlo, P., & Buat, V. 2020, *A&A*, 635, A136
- Bailer-Jones, C. A. L., Fouesneau, M., & Andrae, R. 2019, *MNRAS*, 490, 4, 5615
- Blecha, L., Snyder, G. F., Satyapal, S., & Ellison, S. L. 2018, *MNRAS*, 478, 3, 3056
- Boquien, M., Burgarella, D., Roehly, Y., Buat, V., Ciesla, L., Corre, D., Inoue, A. K., & Salas, H. 2019, *A&A*, 622, A103
- Brunner, H. et al. 2022, *A&A*, 661, A1
- Bruzual, G. & Charlot, S. 2003, *MNRAS*, 344, 4, 1000
- Buat, V., Ciesla, L., Boquien, M., Malek, K., & Burgarella, D. 2019, *A&A*, 632, A79
- Buendia-Rios, T. M., Negrete, C. A., Marziani, P., & Dultzin, D. 2023, *A&A*, 669, A135
- Burgarella, D., Buat, V., & Iglesias-Páramo, J. 2005, *MNRAS*, 360, 4, 1413
- Calderone, G., Nicastro, L., Ghisellini, G., Dotti, M., Sbarrato, T., Shankar, F., & Colpi, M. 2017, *MNRAS*, 472, 4, 4051
- Calzetti, D., Armus, L., Bohlin, R. C., Kinney, A. L., Koornneef, J., & Storchi-Bergmann, T. 2000, *ApJ*, 533, 2, 682
- Chabrier, G. 2003, *PASP*, 115, 809, 763
- Chapin, E. L., Berry, D. S., Gibb, A. G., Jenness, T., Scott, D., Tilanus, R. P. J., Economou, F., & Holland, W. S. 2013, *MNRAS*, 430, 4, 2545
- Ciesla, L., Elbaz, D., & Fensch, J. 2017, *A&A*, 608, A41
- Dey, A. et al. 2019, *AJ*, 157, 5, 168
- Dietrich, M., Appenzeller, I., Vestergaard, M., & Wagner, S. J. 2002, *ApJ*, 564, 2, 581
- Draine, B. T. et al. 2014, *ApJ*, 780, 2, 172
- Duncan, K. J. 2022, *MNRAS*, 512, 3, 3662
- Duras, F. et al. 2017, *A&A*, 604, A67
- Ferrarese, L. & Merritt, D. 2000, *ApJL*, 539, 1, L9
- Gao, F. et al. 2021, *A&A*, 654, A117
- Gao, Z.-K. et al. 2024, arXiv e-prints, arXiv:2405.20616
- Grandi, S. A. 1982, *ApJ*, 255, 25
- Greene, J., Bezanson, R., Ouchi, M., Silverman, J., & the PFS Galaxy Evolution Working Group. 2022, arXiv e-prints, arXiv:2206.14908
- Hashiguchi, A. et al. 2023, *PASJ*, 75, 6, 1246
- Hlavacek-Larrondo, J. et al. 2017, *MNRAS*, 464, 2, 2223
- Holland, W. S. et al. 2013, *MNRAS*, 430, 4, 2513
- Hoshi, A., Yamada, T., & Ohta, K. 2024, *PASJ*, 76, 1, 103
- Inoue, A. K. 2011, *MNRAS*, 415, 3, 2920
- Jenness, T., Cavanagh, B., Economou, F., & Berry, D. S., in R. W. Argyle, P. S. Bunclark, & J. R. Lewis, eds., *Astronomical Data Analysis Software and Systems XVII* (2008), vol. 394 of *Astronomical Society of the Pacific Conference Series*, p. 565
- Kormendy, J. & Ho, L. C. 2013, *ARA&A*, 51, 1, 511
- Kurita, M. et al. 2020, *PASJ*, 72, 3, 48
- Lawrence, A. et al. 2007, *MNRAS*, 379, 4, 1599
- Leitherer, C., Li, I. H., Calzetti, D., & Heckman, T. M. 2002, *ApJS*, 140, 2, 303
- Liddle, A. R. 2004, *MNRAS*, 351, 3, L49
- Lim, C.-F. et al. 2020, *ApJ*, 889, 2, 80
- Liu, T. et al. 2022, *A&A*, 661, A5
- Lyke, B. W. et al. 2020, *ApJS*, 250, 1, 8
- Magorrian, J. et al. 1998, *AJ*, 115, 6, 2285
- Marconi, A. & Hunt, L. K. 2003, *ApJL*, 589, 1, L21
- Markwardt, C. B., in D. A. Bohlender, D. Durand, & P. Dowler, eds., *Astronomical Data Analysis Software and Systems XVIII* (2009), vol. 411 of *Astronomical Society of the Pacific Conference Series*, p. 251
- Martin, D. C. et al. 2005, *ApJL*, 619, 1, L1
- Martínez-Aldama, M. L., del Olmo, A., Marziani, P., Sulentic, J. W., Negrete, C. A., Dultzin, D., D'Onofrio, M., & Perea, J. 2018, *A&A*, 618, A179
- Marziani, P. & Sulentic, J. W. 2014, *MNRAS*, 442, 2, 1211
- Matsubayashi, K. et al. 2019, *PASJ*, 71, 5, 102
- McConnell, N. J. & Ma, C.-P. 2013, *ApJ*, 764, 2, 184
- Merloni, A. et al. 2012, arXiv e-prints, arXiv:1209.3114

- Merloni, A. et al. 2024, *A&A*, 682, A34
- Murakami, H. et al. 2007, *PASJ*, 59, S369
- Narayanan, D. et al. 2010, *MNRAS*, 407, 3, 1701
- Noll, S., Burgarella, D., Giovannoli, E., Buat, V., Marcillac, D., & Muñoz-Mateos, J. C. 2009, *A&A*, 507, 3, 1793
- O'Donnell, J. E. 1994, *ApJ*, 422, 158
- Perrotta, S., Hamann, F., Zakamska, N. L., Alexandroff, R. M., Rupke, D., & Wylezalek, D. 2019, *MNRAS*, 488, 3, 4126
- Petrosian, V. 1976, *ApJL*, 210, L53
- Predehl, P. et al. 2021, *A&A*, 647, A1
- Ricci, C. et al. 2017, *ApJ*, 835, 1, 105
- Richards, G. T. et al. 2015, *ApJS*, 219, 2, 39
- Rowan-Robinson, M. 2000, *MNRAS*, 316, 4, 885
- Rudolf, N., Günther, H. M., Schneider, P. C., & Schmitt, J. H. M. M. 2016, *A&A*, 585, A113
- Runnoe, J. C., Brotherton, M. S., & Shang, Z. 2012, *MNRAS*, 422, 1, 478
- Salvato, M. et al. 2022, *A&A*, 661, A3
- Schlegel, D. J., Finkbeiner, D. P., & Davis, M. 1998, *ApJ*, 500, 2, 525
- Schwarz, G. 1978, *Annals of Statistics*, 6, 2, 461
- Secrest, N. J., Dudik, R. P., Dorland, B. N., Zacharias, N., Makarov, V., Fey, A., Frouard, J., & Finch, C. 2015, *ApJS*, 221, 1, 12
- Shen, Y. 2013, *Bulletin of the Astronomical Society of India*, 41, 1, 61
- Shen, Y. et al. 2024, *ApJS*, 272, 2, 26
- Stalevski, M., Fritz, J., Baes, M., Nakos, T., & Popović, L. Č. 2012, *MNRAS*, 420, 4, 2756
- Stalevski, M., Ricci, C., Ueda, Y., Lira, P., Fritz, J., & Baes, M. 2016, *MNRAS*, 458, 3, 2288
- Stanley, F., Harrison, C. M., Alexander, D. M., Swinbank, A. M., Aird, J. A., Del Moro, A., Hickox, R. C., & Mullaney, J. R. 2015, *MNRAS*, 453, 1, 591
- Suh, H., Civano, F., Trakhtenbrot, B., Shankar, F., Hasinger, G., Sanders, D. B., & Allevalo, V. 2020, *ApJ*, 889, 1, 32
- Symeonidis, M. & Page, M. J. 2018, *MNRAS*, 479, 1, L91
- Takada, M. et al. 2014, *PASJ*, 66, 1, R1
- Toba, Y., Ueda, J., Lim, C.-F., Wang, W.-H., Nagao, T., Chang, Y.-Y., Saito, T., & Kawabe, R. 2018, *ApJ*, 857, 1, 31
- Toba, Y. et al. 2015, *PASJ*, 67, 5, 86
- Toba, Y. et al. 2020a, *ApJ*, 888, 1, 8
- Toba, Y. et al. 2020b, *ApJ*, 899, 1, 35
- Toba, Y. et al. 2020c, *ApJ*, 889, 2, 76
- Toba, Y. et al. 2021a, *ApJ*, 912, 2, 91
- Toba, Y. et al. 2021b, *A&A*, 649, L11
- Toba, Y. et al. 2022a, *PASJ*, 74, 6, 1356
- Toba, Y. et al. 2022b, *A&A*, 661, A15
- Toba, Y. et al. 2024, *ApJ*, 967, 1, 65
- Tody, D., in D. L. Crawford, ed., *Instrumentation in astronomy VI* (1986), vol. 627 of *Society of Photo-Optical Instrumentation Engineers (SPIE) Conference Series*, p. 733
- Véron-Cetty, M. P., Joly, M., & Véron, P. 2004, *A&A*, 417, 515
- Vestergaard, M. & Osmer, P. S. 2009, *ApJ*, 699, 1, 800
- Vestergaard, M. & Wilkes, B. J. 2001, *ApJS*, 134, 1, 1
- Vietri, G. et al. 2018, *A&A*, 617, A81
- Villa-Vélez, J. A., Buat, V., Theulé, P., Boquien, M., & Burgarella, D. 2021, *A&A*, 654, A153
- Wang, W.-H. et al. 2017, *ApJ*, 850, 1, 37
- Wilman, R. J., Fabian, A. C., Crawford, C. S., & Cutri, R. M. 2003, *MNRAS*, 338, 1, L19
- Wright, E. L. et al. 2010, *AJ*, 140, 6, 1868
- Wu, Q., Liao, S., Qi, Z., Luo, H., Tang, Z., & Cao, Z. 2023, *Research in Astronomy and Astrophysics*, 23, 2, 025006
- Wu, Q. & Shen, Y. 2022, *ApJS*, 263, 2, 42
- Yang, G. et al. 2020, *MNRAS*, 491, 1, 740
- Yang, G. et al. 2022, *ApJ*, 927, 2, 192
- York, D. G. et al. 2000, *AJ*, 120, 3, 1579
- Yoshida, M. 2005, *Journal of Korean Astronomical Society*, 38, 2, 117
- Yutani, N., Toba, Y., Baba, S., & Wada, K. 2022, *ApJ*, 936, 2, 118